Digital Camera with Spiral Odd-Symmetry Phase Grating Supports Full-Resolution Computational Refocussing

Patrick R. Gill and David G. Stork
Rambus Labs, 1050 Enterprise Way, Suite 700, Sunnyvale, California, 94089, USA
{*pgill, dstork*} *@rambus.com*

Abstract: Novel odd-symmetry phase gratings produce spatially varying depth-dependent point-spread functions on an imager's sensor plane. The severely blurred sensed image can be inverted computationally to refocus and estimate target distances.

OCIS codes: 090.1970, 110.1758

1. Introduction and background

The problems of automatic digital refocussing and of extending depth of field have received a great deal of study. [1] Extending the depth of field in an imaging system with a fixed f/number beyond the classical geometric limit has been approached through a number of methods in computational imaging. The general approach in point-spread-function engineering is to optically transform or code the sensed optical signal and then digitally process the sensed image. Dowski and Cathy introduced cubic-phase plates, which blurred the image significantly nearly independent of object distance; the sensed image is then digitally sharpened in a space-invariant way, yielding extended depth of field while losing depth information. [2] Ojeda-Castañeda and his colleagues explored different types of lenses and groups of lenses with matched digital processing. [3,4] Cossairt and colleagues introduced special diffusion plates, which blurred the image in an invertible way. [5] Digital refocusing is direct in plenoptic cameras, which capture the four-dimensional light field. [6,7]

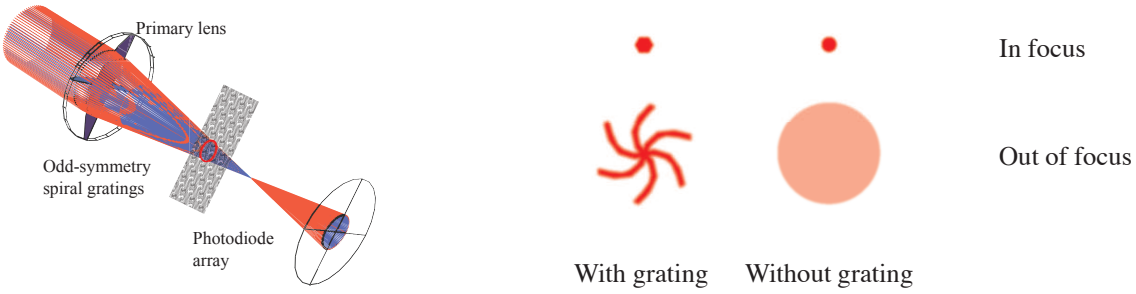

Fig. 1. Left: A ray tracing diagram of a cylinder of rays from a distant point source passing through the primary lens and odd-symmetry spiral gratings onto a photodiode array. (The distance between the gratings and photodiode array is increased just for illustration purposes.) Right: If the grating is not present, the point spread function is small at the conjugate focus (In focus). When the grating is in place a spiral point-spread function results, one covering the spatial-frequency domain (up to the Nyquist limit, and devoid of zeros).

Gill and his colleagues introduced lensless integrated imagers in which wires in traditional CMOS acted as amplitude diffraction gratings. [8–11] Recently, new classes of odd symmetry spiral phase gratings overcame the limitations of those gratings, such as poor low-light sensitivity. [12–14] Here we demonstrate that these novel gratings support computational refocussing and Bayesian depth estimation in a lensed imager.

2. Odd symmetry phase gratings

Figure 2 shows the simulated PSF from a point source of various distances from the primary lens, both with and without the spiral grating. When the point source is at the conjugate focus of the photosensor array (middle figures), the PSFs are small and similar to a standard PSF. However, for point sources at other ranges, the grating induces PSF substructure with high spatial frequency content. This high-frequency content prevents the PSF from being an information-destroying low-pass filter. Note that due to the wavelength- and depth-invariance of odd-symmetry gratings, these patterns are largely wavelength-independent and robust against limited manufacturing precision. [13, 14]

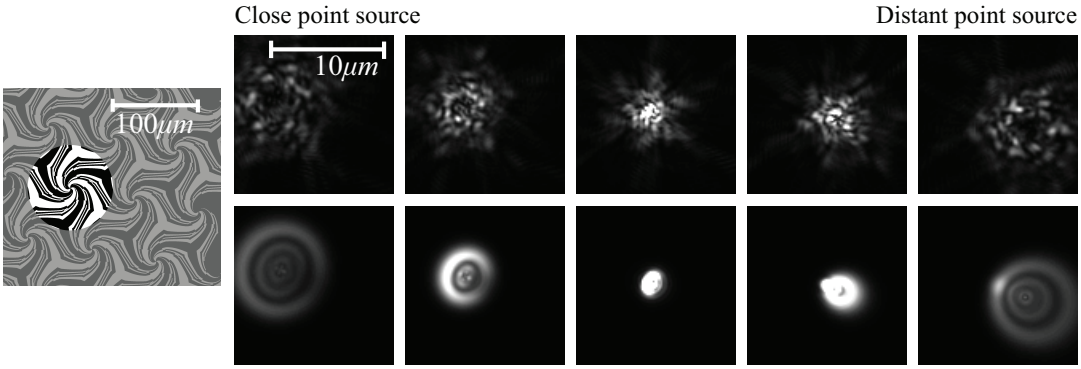

Fig. 2. Effect of phase gratings at different focal depths. Left: Light from a single point source strikes a disk (shown in stark black and white) on an array of spiral odd-symmetry phase gratings. Right, top row: the PSF observable at the sensor array contains computationally-invertible substructure that changes as the point source moves through the conjugate focus of the imager array. Due to the properties of the odd-symmetry grating, these PSFs are wavelength-insensitive. Bottom row: the PSF that would be observed without the phase grating. All simulations assume primary lens aberrations and white light with wavelengths of 400-600 *nm*.

3. Digital refocusing and depth estimation

The most probable object depth $\hat{d}$ at a point in the field of view given sensor data $\mathbf{y}$ can be estimated through Bayesian methods. [15] At each point in the field of view and candidate depth d, one can calculate a candidate image $\mathbf{x} = \mathscr{F}^{-1}\left(\frac{\mathscr{F}(\mathbf{y})}{\mathscr{F}(\mathbf{k}_d)}\right)$, where $\mathbf{k}_d$ is the depth-dependent PSF, and $\mathscr{F}(\cdot)$ and $\mathscr{F}^{-1}(\cdot)$ denote the Fourier transform and its inverse. However, many of these $\mathbf{x}(d,\mathbf{y})$ will be improbable given natural scene statistics, and some ds would even imply negative light intensities in $\mathbf{x}$. By selecting the d that maximizes the product of $p(d)$ and $p(\mathbf{x}(d,\mathbf{y}))$, we can find the most likely depth $\hat{d}$. More formally, let $\mathscr{F}(\mathbf{y}) = \mathscr{F}(\mathbf{x})\mathscr{F}(\mathbf{k}_d) + \mathbf{n}$ where $\mathbf{n}$ is sensor or other noise. The likelihood $p(\mathbf{y}|d)$ equals the probability of the Fourier transform of a scene given $\mathbf{y}$, $\mathbf{n}$ and d: $p(\mathscr{F}(\mathbf{x}(d,\mathbf{y})) + \frac{\mathbf{n}}{\mathscr{F}(\mathbf{k}_d)})$. From this probability we can compute a most-likely depth $\hat{d}$ using Bayes' rule as follows:

$$\hat{d} = \arg\max_d \left[p(d) p\left(\mathscr{F}(\mathbf{x}(d,\mathbf{y})) + \frac{\mathbf{n}}{\mathscr{F}(\mathbf{k}_d)} \right) \right], \tag{1}$$

where the second term incorporates knowledge of the probability distribution of photographed scenes and the noise of the system, all scaled by the (non-zero) Fourier power of the kernel. The high computational complexity of this search over d at each point can be reduced using priors over depth distribution and algorithmic heuristics. With d known, deconvolution with $\mathbf{k}_d$ recovers the in-focus image as well (Fig. 3).

4. Conclusion

We have demonstrated in full, end-to-end simulation that computational imaging systems incorporating odd-symmetry phase gratings can be digitally refocused in a spatially varying manner, thereby extending the depth of field. These methods also yield an estimate of the target depth at each point in the field of view.

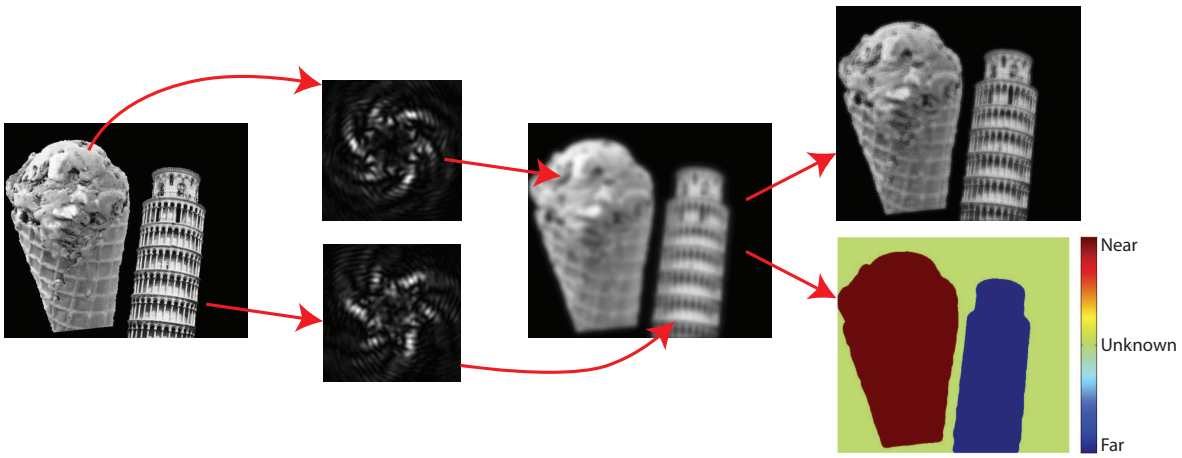

Fig. 3. An end-to-end simulation of the imaging by a lens with our spiral phase grating. At the left is a synthetic image of a close ice cream cone and a distant tower. The corresponding "near" and "far" effective PSFs of each is shown; these produce the final image on the image plane shown at the middle. At the top is a digitally refocussed image and at the bottom the inferred depth map, both computed using the appropriate or "matched" PSF, which would be found using Bayesian methods.

References

1. W. Kesseler and J. Fischer, "Analytical model of autofocus systems with CCD camera," in "Sensors and Camera Systems for Scientific, Industrial, and Digital Photography Applications," , vol. 3965, M. M. Blouke, N. Sampat, G. M. Williams, Jr., and T. Yeh, eds. (SPIE, 2000), vol. 3965, pp. 369–380.
2. E. R. Dowski, Jr. and W. T. Cathey, "Extended depth of field through wave-front coding," Applied Optics **34**, 1859–1866 (1995).
3. A. Castro and J. Ojeda-Castañeda, "Asymmetric phase masks for extended depth of field," Applied Optics **43**, 3474–3479 (2004).
4. J. Ojeda-Castañeda, M. M. Rodríquez, and R. Naranjo, "Tunable phase masks for extended depth of field," in "Progress In Electromagnetics Research Symposium," (Cambridge, MA, 2010), pp. 531–533.
5. O. Cossairt, C. Zhou, and S. Nayar, "Diffusion coded photography for extended depth of field," ACM Transactions on Graphics **29**, 31:1–31:10 (2010).
6. E. H. Adelson and J. Y. Wang, "Single lens stereo with a plenoptic camera," IEEE Transactions on Pattern Analysis and Machine Intelligence **14**, 99–106 (1992).
7. T. Georgiev and A. Lumsdaine, "Depth of field in plenoptic cameras," in "Proceedings of Eurographics," , P. Alliez and M. Magnor, eds. (2009).
8. P. R. Gill, C. Lee, D.-G. Lee, A. Wang, and A. Molnar, "A microscale camera using direct Fourier-domain scene capture," Optics Letters **36**, 2949–2951 (2011).
9. P. R. Gill, C. Lee, S. Sivaramakrishnan, and A. Molnar, "Robustness of planar Fourier capture arrays to colour changes and lost pixels," Journal of Instrumentation **7**, C01–61 (2012).
10. A. Wang and A. Molnar, "A light-field image sensor in 180 *nm* CMOS," IEEE Journal of Solid-State Circuits **47**, 257–271 (2012).
11. A. Wang, P. R. Gill, and A. Molnar, "Light field image sensors based on the Talbot effect," Applied Optics **48**, 5897–5905 (2009).
12. P. R. Gill and D. G. Stork, "Lensless ultra-miniature imagers using odd-symmetry spiral phase gratings," (2013). Submitted for publication.
13. D. G. Stork and P. R. Gill, "Lensless ultra-miniature computational sensors and imagers," in "SensorComm 2013," (Barcelona, Spain, 2013). In press.
14. P. R. Gill, "Odd-symmetry phase gratings produce optical nulls uniquely insensitive to wavelength and depth," submitted for publication (2013). http://arXiv.org/abs/1303.4477.
15. R. O. Duda, P. E. Hart, and D. G. Stork, *Pattern Classification* (Wiley, New York, NY, 2001), 2nd ed.